ORIGINAL ARTICLE

A novel finite element simulation of hot stamping process of DP780 steel based on the Chaboche thermomechanically hardening model

Hamid Hajbarati[1] · Asghar Zajkani[1]

Abstract

Advanced high-strength steels (AHSS) despite excellent properties with low weight and high strength have the concern of high springback occurrence. The amount of springback can be reduced by hot forming process. In this paper, the influence of temperature rises on the springback quantities generated potentially during a hot stamping process of the DP780 steel is investigated. To obtain a proper description for hardening behavior, a type of the Chaboche thermomechanically constitutive model has been used in conjunction with an anisotropic Yld2000-2D yield criterion. Since the elastic modulus of the AHSS during loading and unloading stages can make considerable influences on the springback, consideration of Young's modulus as a function of equivalent plastic strain is necessary. Moreover, the process is simulated via ABAQUS software implementing UMAT and VUMAT user-defined subroutines as well as the forward Euler explicit integration scheme is applied to calculate the stress and strain at the end of time increments. The results demonstrate the efficiency of the novel temperature-dependent Chaboche model to predict the level of stresses and temperature during and after hot stamping process.

Keywords Temperature-dependent Chaboche model · Hot stamping · Springback · Advanced high-strength steel · Finite element simulation

1 Introduction

Nowadays, particular characteristics of advanced high-strength steel (AHSS) alloys due to their high strength and low weight have motivated engineering to apply them in different apparatuses. In the past decade, these interests have been rapidly grown up in such a way that a large number of researchers have investigated different mechanical aspects of these alloys. Recently, Martínez-Palmeth et al. [1] presented an experimental and numerical analysis of the formability of high-strength H240LA steel sheets. Also, Zhang et al. [2] introduced an inverse identification of the post-necking work hardening behavior of thick HSS through full-field strain measurements during diffuse necking. Experimental response of high-strength steels to localized blast loading is given in [3]. He et al. [4] expressed a rate and temperature-dependent unified creep-plasticity model. They reported the temperature

function, drag stress evolution function, and the adjustment equations to be determined. On contrary, one of the disadvantages of these alloys is its high springback which is arisen from the Bauschinger effect of hardening mechanisms during forward loading and reverse unloading processes [5]. Some general-related considerations around the Bauschinger effect can be found in the work done by [6] as well as the references inside it. Today, the warm or hot forming processes are used to reduce the springback phenomenon in these alloys. The hot forming process is used for molds with different shapes [7]. In the following, we will have a look at the hot forming processes for U-shaped deep draw bending and hot stamping. In the field of the U-shaped deep drawing process, a lot of researches have been done in recent years [8]. On the other hand, Mori et al. [9] developed a warm and hot stamping process of ultra-high tensile strength steel sheets by using a resistance heating to improve springback and formability. Also, the effects of the heating temperature on the springback and formability of ultra-high tensile strength steel sheets were examined. The results showed that the springback of the high tensile strength steel sheets eliminate by heating the sheet.

Yanagimoto et al. [10] investigated the springback of high-strength steel after hot and warm sheet forming to evaluate the

✉ Asghar Zajkani
zajkani@eng.ikiu.ac.ir

[1] Department of Mechanical Engineering, Imam Khomeini
International University, Qazvin, Iran

Table 1 Material parameters of the temperature-dependent Chaboche model [30]

Parameters	k_{c1}	m_{c1}	$k_{\gamma1}$	$m_{\gamma1}$	k_{c2}	m_{c2}	$k_{\gamma2}$	$m_{\gamma2}$	k_{R0}	m_{R0}	k_{Rs}
Unit	MPa	MPa/K	-	/K	MPa	MPa/K	-	/K	MPa	MPa/K	MPa
Values	22,569	29.8	128	0.21	461.41	1.72	0	0	445	− 0.76	186.04

effect of forming temperature on the amount of springback and showed that the springback is markedly reduced when the forming temperature is higher than 750 K. Moreover, Naderi et al. [11] studied the hot stamping of 22MnB5 boron steel sheets by using a water or nitrogen cooling media. Also, the evolution of the temperature and force were simulated during the hot stamping process by using a coupled thermomechanical FEM program. They concluded that die cooling media has a significant effect on the material properties after hot stamping. Xing et al. [12] proposed a material model based on experimental data of mechanics and thermal physical properties, and used it for hot stamping condition of quenchable steel and performed the numerical simulation of hot forming, quenching, and springback with the ABAQUS software. The obtained results showed that the springback of

hot stamping parts increases when the blank holder force decreases; it increases when the clearance between the punch and dies increases and when the die radius increases. Liu et al. [13] investigated the flow behavior of the 22MnB5 AHSS through hot tensile tests. They build a finite element model of the hot stamping process for the shaped part by the ABAQUS/Explicit to investigate the influence of blank holder force and die gap on the hot forming process. Obtained results showed that large blank holder force reduces the amount of springback, and die gap has a considerable influence on the distribution of temperature on the side wall. Worswick et al. [14] carried out both experimental and numerical considerations for hot stamped axial crush members with a non-tailored and three-tailored configurations as one-half of the rail was quenched while the other formed half was heated
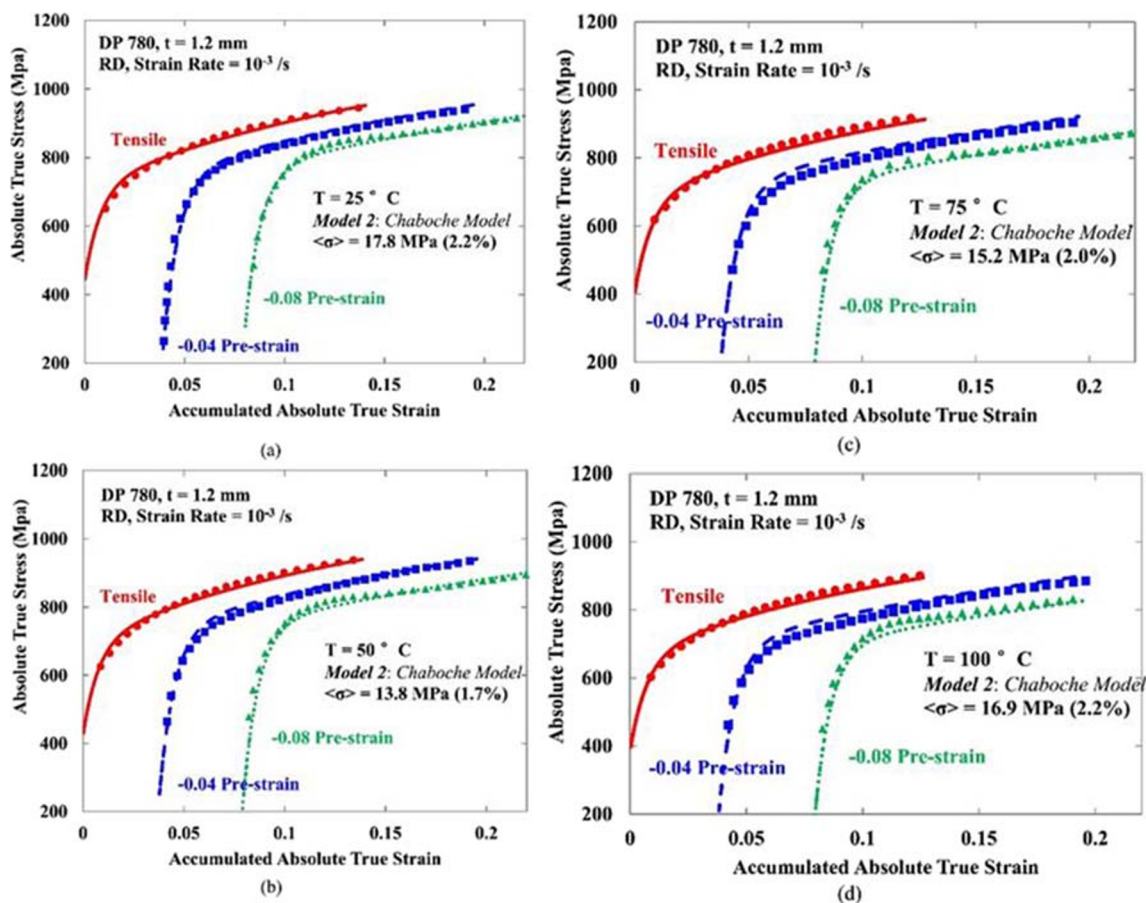

Fig. 1 Comparisons of the experimental data and Chaboche model for tensile and CT tests at each tested temperature for DP780. **a** 25 °C. **b** 50 °C. **c** 75 °C. **d** 100 °C (adapted from [30])

Table 2 Parameters of the Yld2000-2d yield criterion

Parameter	a_1	a_2	a_3	a_4	a_5	a_6	a_7	a_8
Value	0.9276	1.0243	0.9622	0.9880	1.0043	0.9165	1.0043	1.0324

during several temperatures. Liu et al. [15] performed several tensile tests to examine the flow stress of the material HSS 22MnB5 at different strains, strain rates, and temperatures. They carried out material modeling and FE numerical simulations to investigate the effect of the processing parameters on the hot forming process and they concluded that springback is mainly caused by different cooling rates, and the nonhomogeneous shrink of material during the hot forming process and the creep strain is the main factor influencing the amount of the springback. Lee et al. [16] performed the U-draw/bending experiments of DP and TRIP steel sheets and presented particular simulations to investigate the characteristics of springback in sheet metals and used the finite element method for the simulation of springback. The obtained results showed that the springback predictions were greatly influenced by the choice of the hardening model but slightly affected by the choice of the yield criterion.

In the case of the semi-analytical model to predict springback of metallic parts, several studies have been done in recent years [17]. In addition, Heller and Kleiner [18] developed a mathematical model to make a fast semi-analytical simulation of the air bending process of thin and thick sheets. The mathematical description of the shift of individual fibers and the changes of thickness has been considered. This novel model can be used in practical cases and where the numerical method cannot be used. Lee et al. [19] introduced a simplified hybrid technique to anticipate springback in a 2D draw bend test considering the bending effects of membrane. The model can accommodate general anisotropic yield functions along

with nonlinear isotropic-kinematic hardening under the plane strain condition. Also, for validation purposes, the results were compared with experiments. Panthi and Ramakrishnan [20] proposed a phenomenological model to explore an arc bending process by means of the deformation energy approach and compared with experimental and FE results. Le Quilliec et al. [21] presented a semi-analytical model for large strain analysis of sheet metal forming under plane strain bending and tension. In that work, the loading is assumed to be distributed homogeneously in the length direction. The semi-analytical model is applied to standard test cases and then compared with full-scale simulations. Also, the springback behavior of 3D tubes was proposed by [22] by approximating its deformation through a theoretical discretization for stress distributions and residual deformations. Then, a new method was applied for springback prediction in a typical 3D tube by demonstrating a remarkable agreement between theoretical and experimental results.

In previous articles, the authors investigated analytically the effect of hardening parameters, mechanical condition, pre-strain, and variable unloading modulus on springback in U-draw bending process of DP780 steel [23–25].

In this paper, a novel finite element model is presented to predict springback behavior of DP780 steel sheets during and after the hot stamping process based on a temperature-dependent Chaboche hardening model and Yld2000-2d yield function. The ABAQUS software is used to simulate the forming process stages via the forward Euler explicit integration scheme and plane strain condition. Furthermore, UMAT

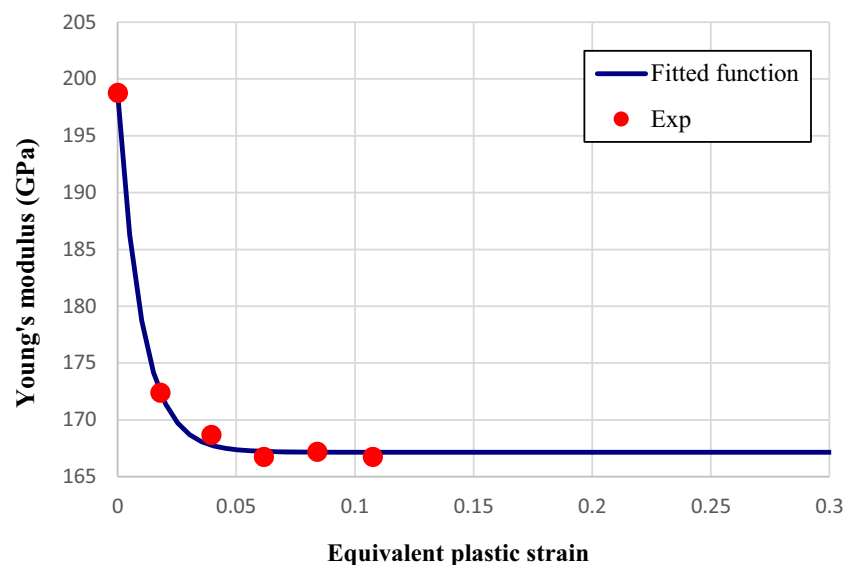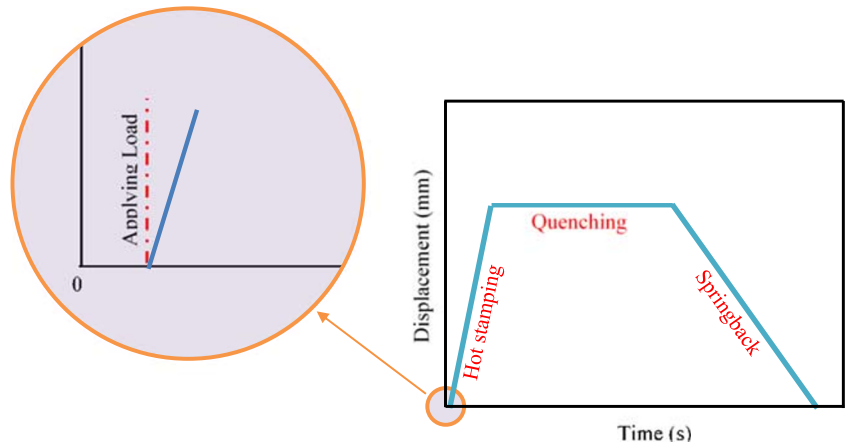**Fig. 2** The relation between Young's modulus and plastic strain during the uniaxial loading

Fig. 3 Forming steps and movement of the punch during the hot stamping process (adapted from [13])

and VUMAT user subroutines are used in order to define the material behavior. Finally, the hot stamping process of DP780 steel is simulated based on these models and algorithms.

2 Theory

2.1 Temperature-dependent Chaboche hardening model

In the case of a combined isotropic-kinematic hardening model, the yield function can be expressed with:

$$F = \overline{\sigma}(\boldsymbol{\sigma} - \boldsymbol{X}) - R - \sigma_y = 0 \tag{1}$$

where $\boldsymbol{\sigma}$ is the Cauchy stress tensor, σ_y is the initial yield stress, and $\boldsymbol{X}$ is the back stress tensor which indicates the yield surface transition. Also, R is the size of yield surface which develops through isotropic hardening and $\overline{\sigma}$ is the equivalent stress.

Back stress vector can be composed of n components, which each part changes with its own law as follows [26]:

$$X = \sum_{i=1}^{n} X_i \tag{2}$$

In the Chaboche hardening model, each part of back stress tensor develops according to the Armstrong and Frederick law [27] as follow:

$$dX_i = c_i d\varepsilon^p - \gamma_i X_i d\overline{\varepsilon}^{\mathrm{p}} \tag{3}$$

where $d\varepsilon^p$ is the plastic strain increment, $d\overline{\varepsilon}^p$ is the equivalent plastic strain increment, and the parameters c_i and γ_i are the material constants. The first part in Eq. (3) is suggested by Prager [28], which represents linear kinematic hardening. The second phrase in Eq. (3) represents a nonlinear revolution which develops through isotropic hardening for a non-proportional strain. With these statements, the Chaboche hardening model is able to capture the Bauschinger effect and transient behavior during yield process in large strains. Since this model is not able to model permanent softening, the second phrase in one part of back stress tensor should be eliminated. Several isotropic-kinematic hardening rules are compared with the Armstrong-Frederick and Chaboche hardening criteria by Karvan and Farahani [29]. The framework of hardening rules was constructed on the basis of viscoplasticity constitutive equation to account for the effects of stress rate and time dependency.

Fig. 4 Definition of geometrical and thermal surfaces and contact pairs
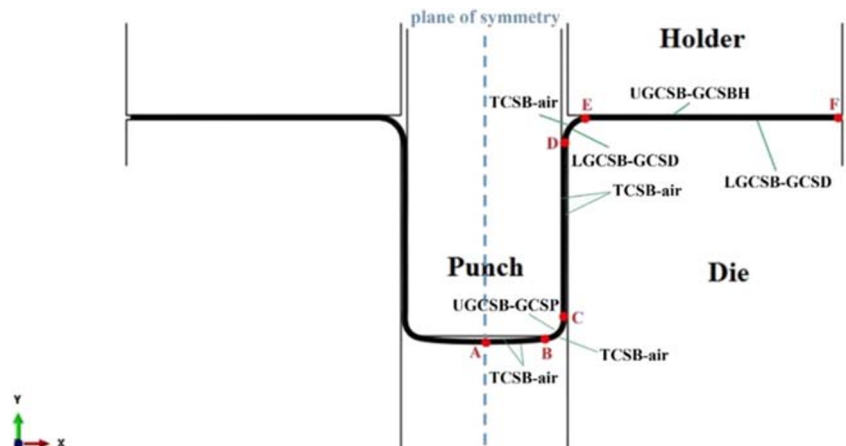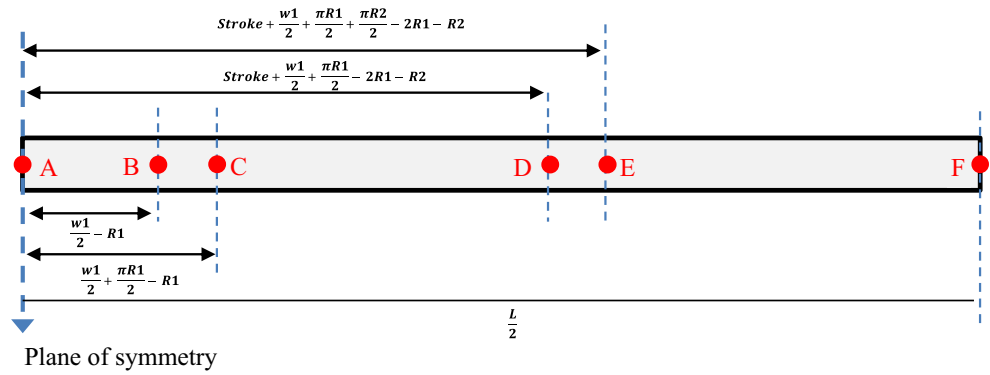
Fig. 5 The position of contact surfaces border in undeformed blank

$Stroke + \frac{w1}{2} + \frac{\pi R1}{2} + \frac{\pi R2}{2} - 2R1 - R2$

$Stroke + \frac{w1}{2} + \frac{\pi R1}{2} - 2R1 - R2$

A   B   C   D   E   F

$\frac{w1}{2} - R1$

$\frac{w1}{2} + \frac{\pi R1}{2} - R1$

$\frac{L}{2}$

Plane of symmetry

The Chaboche hardening model uses a saturated function for isotropic hardening as follows:

$$dR = b(R_s - R)d\bar{\varepsilon}^p \tag{4}$$

where R and R_s are the current and final size of the yield surface and b is the material constant. The size of the yield surface increases with equivalent plastic strain and saturates to R_s value.

The constants of the Chaboche model can be obtained with tension-compression tests. In order to obtain the constants during uniaxial loading, the following equations obtained from Eq. (3) integrating will be used in one direction:

$$X = \frac{3}{2}\upsilon\frac{c}{\gamma} + \left(X_0 - \frac{3}{2}\upsilon\frac{c}{\gamma}\right)e^{-\gamma(\bar{\varepsilon}^p - \bar{\varepsilon}_0^p)} \tag{5}$$

where $\upsilon = \pm 1$ represents the flow direction, $\bar{\varepsilon}_0^p$ and X_0 represent the amount of pre-strain and initial reverse flow stress, respectively.

Also, the isotropic hardening can be represented by the following equation:

$$R = R_o + R_s(1 - e^{-b\bar{\varepsilon}^p}) \tag{6}$$

where R_o is the yield stress and $R_o + R_s$ is the saturated stress value at large strains.

The temperature affects the Chaboche model in two cases, on the size of yield surface (isotropic hardening) and back stress change (non-isotropic hardening). The evolution of size and location of yield surface with respect to temperature (T) can be expressed as [30]:

$$d\mathbf{X}_i = c_i(T)d\varepsilon^p - \gamma_i(T)X_i d\bar{\varepsilon}^p + \frac{1}{c_i(T)}\frac{\partial c_i(T)}{\partial T}X_i dT \tag{7}$$

$$dR = b(T)(R_s(T) - R)d\bar{\varepsilon}^p \tag{8}$$

In comparison with Eq. (3), there is a temperature-dependent back stress in Eq. (7) in order to obtain an independent temperature micro-structure hardening model. Also, the parameters R_s, R_o, C_1, C_2, and γ_1 can be described based on a linear function of temperature as follows:

$$\xi_i = k_{\xi_i} + m_{\xi_i}(T - T_R) \qquad i = 1.2.\ldots.6 \tag{9}$$

where $\xi_i (i = 1.2. \ldots.6)$ is the coefficients R_s, R_o, C_1, C_2, γ_1, b, and T_R is the room temperature. The temperature coefficients k_{ξ_i} and m_{ξ_i} for each Chaboche coefficient are listed in Table 1.

The differences between experimental data and the Chaboche model are shown in Fig. 1.

2.2 Barlat's Yld2000-2d yield function

The non-quadratic anisotropic yield function Yld2000-2d has the following form [31]:

$$\Phi(\sigma, X) = \phi' + \phi'' - 2\bar{\sigma}^m = 0 \tag{10}$$

where :

$$\phi' = \left|S_1' - S_2'\right|^m \text{ and } \phi'' = \left|2S_2'' + S_1''\right|^m + \left|2S_1'' + S_2''\right|^m \tag{11}$$
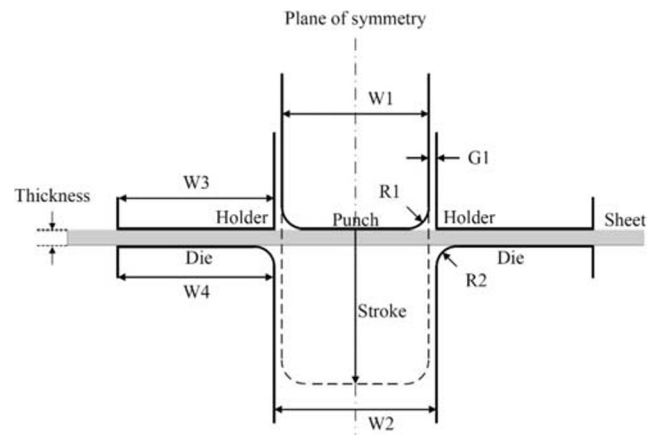
Fig. 6 Schematic view of tools and their dimensions for the 2D draw-bending test

Table 3 Dimensions for the 2D draw-bending test

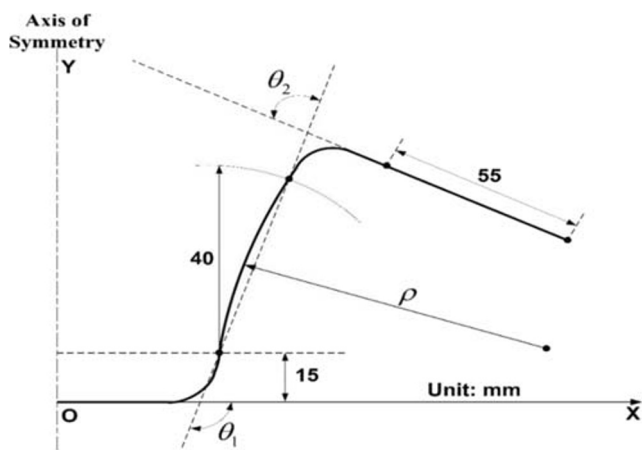| Parameters	W1	W2	W3	W4	R1	R2	G1	Stroke
Dimensions (mm)	50.0	54.0	89.0	89.0	5.0	7.0	2.0	71.8

Fig. 7 Schematic of springback measurement method

where S' and S'' are the linearly transformed stress tensors and the subscripts 1 and 2 are their principal values. The transformations of the Cauchy stress σ into S' and S'' involve two linear transformations:

$$S' = C's = C'T\sigma = L'\sigma \tag{12a}$$

$$S'' = C''s = C''T\sigma = L''\sigma \tag{12b}$$

The transformation T calculates the deviatoric stress s and other transformations C' and C'' induce anisotropy. The products of the two transformations are represented as L' and L'' which can be expressed in matrix form as below:

$$\begin{bmatrix} S'_{xx} \\ S'_{yy} \\ S'_{xy} \end{bmatrix} = \begin{bmatrix} L'_{11} & L'_{12} & 0 \\ L'_{21} & L'_{22} & 0 \\ 0 & 0 & L'_{66} \end{bmatrix} \begin{bmatrix} \sigma_{xx} \\ \sigma_{yy} \\ \sigma_{xy} \end{bmatrix} \tag{13a}$$

$$\begin{bmatrix} S''_{xx} \\ S''_{yy} \\ S''_{xy} \end{bmatrix} = \begin{bmatrix} L''_{11} & L''_{12} & 0 \\ L''_{21} & L''_{22} & 0 \\ 0 & 0 & L''_{66} \end{bmatrix} \begin{bmatrix} \sigma_{xx} \\ \sigma_{yy} \\ \sigma_{xy} \end{bmatrix} \tag{13b}$$

$$\begin{bmatrix} L'_{11} \\ L'_{12} \\ L'_{21} \\ L'_{22} \\ L'_{66} \end{bmatrix} = \begin{bmatrix} 2/3 & 0 & 0 \\ -1/3 & 0 & 0 \\ 0 & -1/3 & 0 \\ 0 & 2/3 & 0 \\ 0 & 0 & 1 \end{bmatrix} \begin{bmatrix} a_1 \\ a_2 \\ a_7 \end{bmatrix} \tag{14a}$$

$$\begin{bmatrix} L''_{11} \\ L''_{12} \\ L''_{21} \\ L''_{22} \\ L''_{66} \end{bmatrix} = \frac{1}{9} \begin{bmatrix} -2 & 2 & 8 & -2 & 0 \\ 1 & -4 & -4 & 4 & 0 \\ 4 & -4 & -4 & 1 & 0 \\ -2 & 8 & 2 & -2 & 0 \\ 0 & 0 & 0 & 0 & 9 \end{bmatrix} \begin{bmatrix} a_3 \\ a_4 \\ a_5 \\ a_6 \\ a_8 \end{bmatrix} \tag{14b}$$

The value of anisotropy coefficients a_1–a_8 are given in Table 2. For the yield function exponent, $m = 6$ is recommended for BCC and $m = 8$ for FCC materials.

Table 4 Parameters used in hot stamping simulation

Geometrical parameters of blank	Length	360 mm
	Width	30 mm
	Thickness	1.4 mm
Coefficient of friction		0.1
Temperature of air		25 °C
Density		7800 kg/m^3
Poisson's ratio		0.3

2.3 Variable elastic modulus

Elastic modulus can be considered as a function of equivalent plastic strain using the experimental data of Numisheet 2011 with a function proposed by [32] as follows:

$$E\left(\overline{\varepsilon}^p\right) = E_0 - (E_0 - E_a)\left(1 - e^{-\xi\overline{\varepsilon}^p}\right) \tag{15}$$

where E_a, E_0, and ξ in the above equation are respectively the saturated Young's modulus, initial young modulus, and the material parameter as shown in Fig. 2. It can be seen that by increasing the plastic strain, the elastic modulus decreases to reach the finally saturated value (E_a). The parameters E_0, E_a, and ξ in Eq. (15) are respectively equal to 198.8 GPa, 167.15 GPa, and 99.55 [33]. Here, we assumed that material elastic modulus is constant and has no change with temperature.

3 Forward Euler explicit integration scheme

According to the associated flow rule, we have:

$$d\varepsilon^p = d\lambda \frac{\partial \Phi}{\partial \sigma} \tag{16}$$

where $d\lambda$ is the plastic multiplier. According to the plastic work formulation:

$$dw^p = (\sigma - X) : d\varepsilon^p = \overline{\sigma} d\overline{\varepsilon}^p \tag{17}$$

where $d\overline{\varepsilon}^p$ is the increment of the equivalent plastic strain.

Using the Euler theorem for the homogeneous, the yield function Φ is a homogeneous function of degree m as follows:

$$\frac{\partial \Phi}{\partial \sigma} : (\sigma - X) = 2m\overline{\sigma}^m \tag{18}$$

The strain increment can be decomposed to the elastic component and plastic component as follows:

$$d\varepsilon = d\varepsilon^e + d\varepsilon^p \tag{19}$$

Table 5 The comparison between the results obtained from the experiment and present FEM method at room temperature

Parameter	θ_1(degree)	θ_2 (degree)	ρ (mm)
Experimental [33]	115.8	79.2	118.2
Simulation (present model)	113	79	80
Error %	2.41	0.25	32.32

According to the plastic work formulation and the Euler's theory for the homogenous functions, the equivalent plastic strain increment can be achieved as follows:

$$d\bar{\varepsilon}^p = 2m\bar{\sigma}^{m-1}d\lambda \tag{20}$$

According to the Hooke's law, the Cauchy stress is a proportional elastic strain as follows:

$$d\boldsymbol{\sigma} = \mathbf{C}^e : d\boldsymbol{\varepsilon}^e = \mathbf{C}^e : (d\boldsymbol{\varepsilon} - d\boldsymbol{\varepsilon}^p) \tag{21}$$

where $\mathbf{C}^e$ is the second-order elasticity tensor. According to the consistency condition during the plastic deformation, the Cauchy stress should stay on the yield surface which leads to the following relation:

$$d\boldsymbol{\Phi} = \frac{\partial \boldsymbol{\Phi}}{\partial \boldsymbol{\sigma}} : (d\boldsymbol{\sigma} - d\mathbf{X}) + \frac{\partial \boldsymbol{\Phi}}{\partial \bar{\varepsilon}^p} d\bar{\varepsilon}^p = 0 \tag{22}$$

Substituting Eqs. (7), (20), and (21) into Eq. (22) and after some manipulation, it can be written as:

$$\frac{\partial \boldsymbol{\Phi}}{\partial \boldsymbol{\sigma}} : \left(\mathbf{C}^e : (d\boldsymbol{\varepsilon} - d\boldsymbol{\varepsilon}^p) - \sum_{i=1}^{2} \left(c_i(T)d\boldsymbol{\varepsilon}^p - \gamma_i(T)\mathbf{X}_i d\bar{\varepsilon}^p + \frac{1}{c_i(T)}\frac{\partial c_i(T)}{\partial T}\mathbf{X}_i dT \right) \right) - 2m\bar{\sigma}^{m-1}b(T)(R_s(T) - R)d\bar{\varepsilon}^p = 0 \tag{23}$$

Substituting Eq. (20) in the above equation, it can be re-arranged as follows:

$$\frac{\partial \boldsymbol{\Phi}}{\partial \boldsymbol{\sigma}} : \left(\mathbf{C}^e : \left(d\boldsymbol{\varepsilon} - d\lambda\frac{\partial \boldsymbol{\Phi}}{\partial \boldsymbol{\sigma}} \right) - \sum_{i=1}^{2} \left(c_i(T)d\lambda\frac{\partial \boldsymbol{\Phi}}{\partial \boldsymbol{\sigma}} - 2m\gamma_i(T)\mathbf{X}_i\bar{\sigma}^{m-1}d\lambda + \frac{1}{c_i(T)}\frac{\partial c_i(T)}{\partial T}\mathbf{X}_i dT \right) \right) - 4m^2 b(T)(R_s(T) - R)\bar{\sigma}^{2(m-1)}d\lambda$$

$$= 0 \tag{24}$$

Therefore, according to the above equation, the plastic multiplier can be defined as follows:

$$d\lambda = \frac{\dfrac{\partial \boldsymbol{\Phi}}{\partial \boldsymbol{\sigma}} : \left(\mathbf{C}^e : d\boldsymbol{\varepsilon} - \sum_{i=1}^{2}\left(\dfrac{1}{c_i(T)}\dfrac{\partial c_i(T)}{\partial T}\mathbf{X}_i dT \right) \right)}{\dfrac{\partial \boldsymbol{\Phi}}{\partial \boldsymbol{\sigma}} : \left(\mathbf{C}^e : \dfrac{\partial \boldsymbol{\Phi}}{\partial \boldsymbol{\sigma}} + \sum_{i=1}^{2}\left(c_i(T)\dfrac{\partial \boldsymbol{\Phi}}{\partial \boldsymbol{\sigma}} - 2m\gamma_i(T)\mathbf{X}_i\bar{\sigma}^{m-1} \right) \right) + 4m^2 b(T)(R_s(T) - R)\bar{\sigma}^{2(m-1)}} \tag{25}$$

Substituting the above equation into Eq. (21) leads to obtain the following equation:

$$d\boldsymbol{\sigma} = \mathbf{C}^e : \left(d\boldsymbol{\varepsilon} - \frac{\dfrac{\partial \boldsymbol{\Phi}}{\partial \boldsymbol{\sigma}}\left(\dfrac{\partial \boldsymbol{\Phi}}{\partial \boldsymbol{\sigma}} : \mathbf{C}^e \right) : d\boldsymbol{\varepsilon} - \dfrac{\partial \boldsymbol{\Phi}}{\partial \boldsymbol{\sigma}}\left(\dfrac{\partial \boldsymbol{\Phi}}{\partial \boldsymbol{\sigma}} : \sum_{i=1}^{2}\left(\dfrac{1}{c_i(T)}\dfrac{\partial c_i(T)}{\partial T}\mathbf{X}_i dT \right) \right)}{\dfrac{\partial \boldsymbol{\Phi}}{\partial \boldsymbol{\sigma}} : \left(\mathbf{C}^e : \dfrac{\partial \boldsymbol{\Phi}}{\partial \boldsymbol{\sigma}} + \sum_{i=1}^{2}\left(c_i(T)\dfrac{\partial \boldsymbol{\Phi}}{\partial \boldsymbol{\sigma}} - 2m\gamma_i(T)\mathbf{X}_i\bar{\sigma}^{m-1} \right) \right) + 4m^2 b(T)(R_s(T) - R)\bar{\sigma}^{2(m-1)}} \right) \tag{26}$$

The stress increment can be defined as follows:

$$d\boldsymbol{\sigma} = \mathbf{C}^{ep}d\boldsymbol{\varepsilon} + \frac{\left(\mathbf{C}^e : \frac{\partial \Phi}{\partial \boldsymbol{\sigma}}\right) \otimes \left(\frac{\partial \Phi}{\partial \boldsymbol{\sigma}} : \Sigma_{i=1}^2 \left(\frac{1}{c_i(T)}\frac{\partial c_i(T)}{\partial T}\mathbf{X}_i dT\right)\right)}{\frac{\partial \Phi}{\partial \boldsymbol{\sigma}} : \left(\mathbf{C}^e : \frac{\partial \Phi}{\partial \boldsymbol{\sigma}} + \Sigma_{i=1}^2 \left(c_i(T)\frac{\partial \Phi}{\partial \boldsymbol{\sigma}} - 2m\gamma_i(T)\mathbf{X}_i\overline{\sigma}^{m-1}\right)\right) + 4m^2 b(T)(R_s(T) - R)\overline{\sigma}^{2(m-1)}} \tag{27}$$

where the tangential elastoplastic stiffness matrix can be written as:

$$\mathbf{C}^{ep} = \mathbf{C}^e - \frac{\left(\mathbf{C}^e : \frac{\partial \Phi}{\partial \boldsymbol{\sigma}}\right) \otimes \left(\mathbf{C}^e : \frac{\partial \Phi}{\partial \boldsymbol{\sigma}}\right)}{\frac{\partial \Phi}{\partial \boldsymbol{\sigma}} : \mathbf{C}^e : \frac{\partial \Phi}{\partial \boldsymbol{\sigma}} + \frac{\partial \Phi}{\partial \boldsymbol{\sigma}} : \Sigma_{i=1}^2 \left(c_i(T)\frac{\partial \Phi}{\partial \boldsymbol{\sigma}} - 2m\gamma_i(T)\mathbf{X}_i\overline{\sigma}^{m-1}\right) + 4m^2 b(T)(R_s(T) - R)\overline{\sigma}^{2(m-1)}} \tag{28}$$

In the case of the plane strain condition, the elastic stiffness matrix can be defined as:

Fig. 8 a The final shape of the plate after springback at room temperature. b Experimental and predicted springback profiles after U-draw bending at room temperature
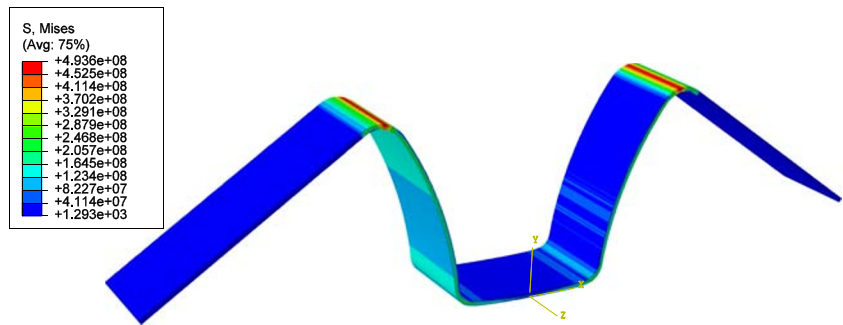
(a)
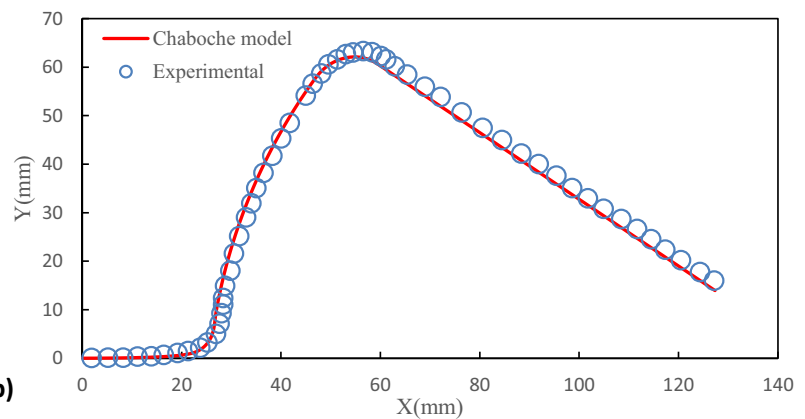
(b)

Fig. 9 Distribution of temperature for heating temperature (**a**) $T_h = 100\ °C$, (**b**) $T_h = 200\ °C$, (c) $T_h = 300\ °C$, (d) $T_h = 400\ °C$ after quenching and before springback
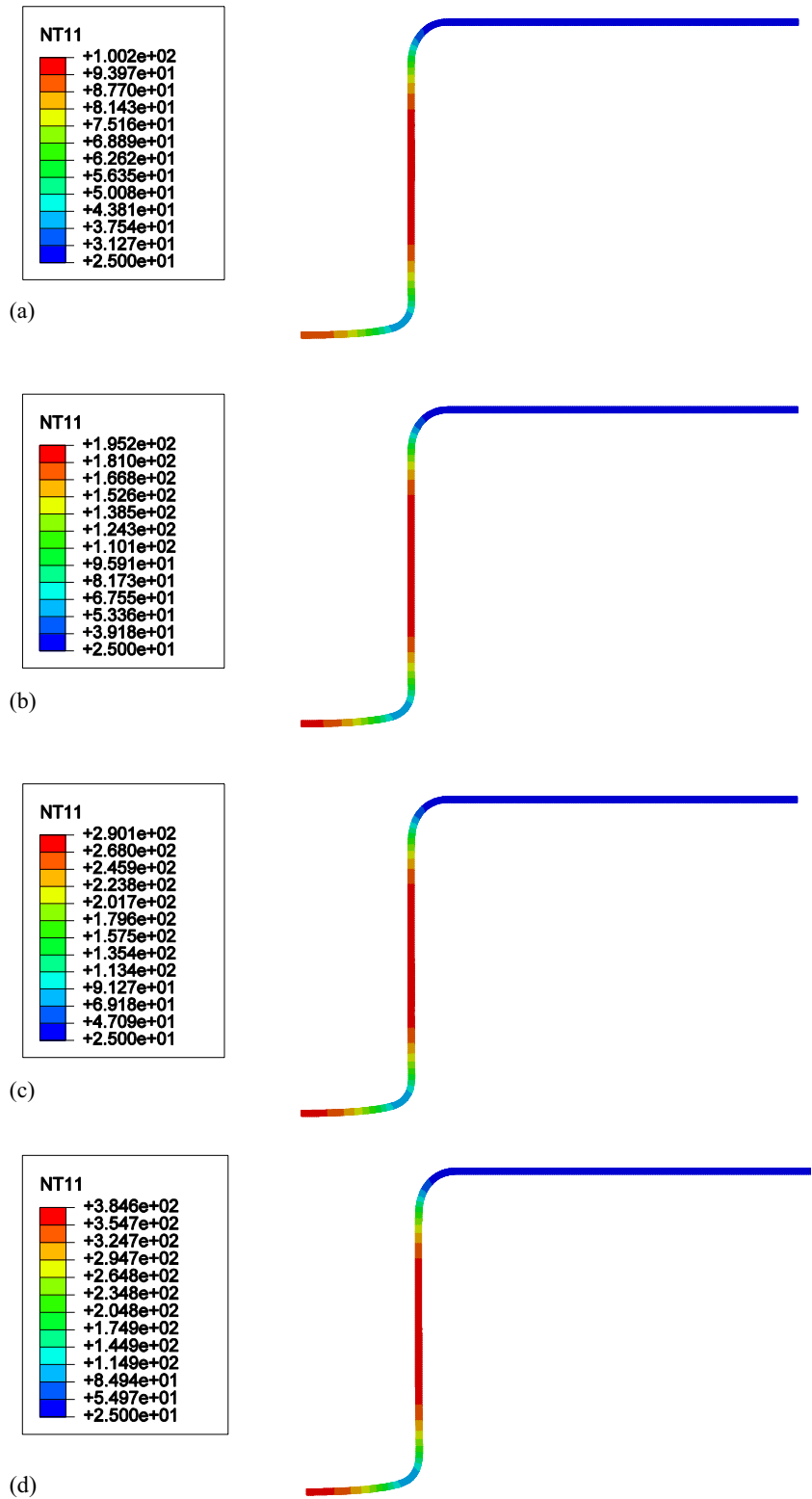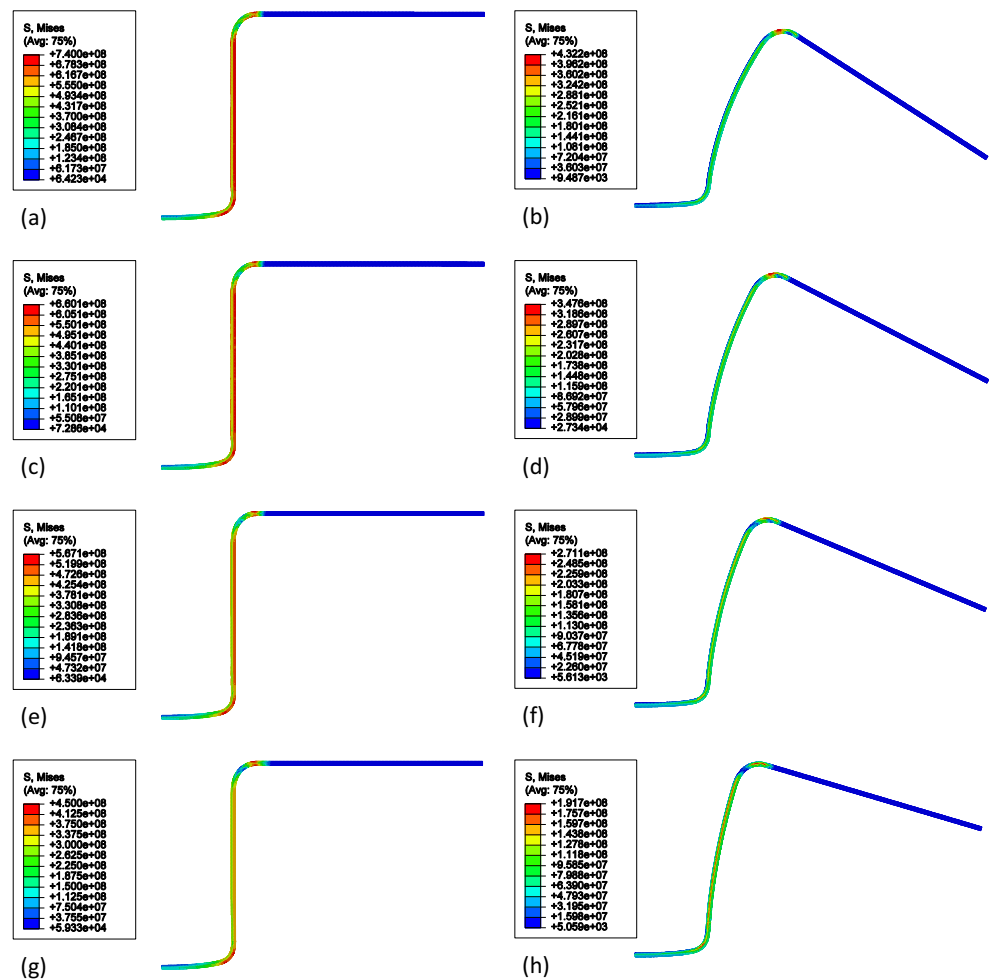
Fig. 10 Distribution of stress for different values of initial hot temperature after quenching (**a**) $T_h = 100\ °C$, (**c**) $T_h = 200\ °C$, (**e**) $T_h = 300\ °C$, (**g**) $T_h = 400\ °C$; and after springback (**b**) $T_h = 100\ °C$, (**d**) $T_h = 200\ °C$, (**f**) $T_h = 300\ °C$, (**h**) $T_h = 400\ °C$

$$
\begin{bmatrix} \sigma_{xx} \\ \sigma_{yy} \\ \tau_{xy} \end{bmatrix} = \frac{E}{(1+\nu)(1-2\nu)} \begin{bmatrix} 1-\nu & \nu & 0 \\ \nu & 1-\nu & 0 \\ 0 & 0 & \frac{1-2\nu}{2} \end{bmatrix} \begin{bmatrix} \varepsilon_{xx} \\ \varepsilon_{yy} \\ \gamma_{xy} \end{bmatrix}
$$
(29)

Here, a forward Euler explicit integration scheme is applied to calculate the stress and strain increment. The plastic strain and back stress can be updated with:

$$
\boldsymbol{\varepsilon}^{t+\Delta t} = \boldsymbol{\varepsilon}^{t} + d\lambda \frac{\partial \Phi}{\partial \boldsymbol{\sigma}}
$$
(30)

$$
\mathbf{X}_i^{t+\Delta t} = \mathbf{X}_i^{t} + \Delta \mathbf{X}_i
$$
(31)

$$
\mathbf{X}^{t+\Delta t} = \mathbf{X}^{t} + \Delta \mathbf{X}
$$
(32)

The stress at the end of time increment can be obtained based on the Hook's law as follows:

$$
\boldsymbol{\sigma}^{t+\Delta t} = \boldsymbol{\sigma}^{t} + \mathbf{C}^e(d\boldsymbol{\varepsilon} - d\boldsymbol{\varepsilon}^p)
$$
(33)

4 FE numerical simulation steps

The movement of the punch during the hot stamping process is shown in Fig. 3. It can be seen that there is 4 basic steps which are the following: (a) applying the blank holder force on the blank, (b) move the punch down and forming the blank while the holder and die are stationary, (c) quenching the part which during this process the temperature decreases, (d) springback process which punch moves up and the stresses are released. According to these steps, the U-shaped hot stamping process consist of these computational steps, i.e., (a) applying the blank holder force, (b) numerical simulation of the hot forming process, (c) numerical simulation of the cooling, (d) numerical computation of the springback. Time spans used in each step are as follows: 0.0001 s in applying blank holder force, 0.9 s in hot stamping analysis, 6 s in quenching step, and 3.8 s in analysis of springback [13].

5 Determination of thermal constants

In order to have accurate thermomechanical FE simulation of the hot stamping process, some thermal constants are needed.
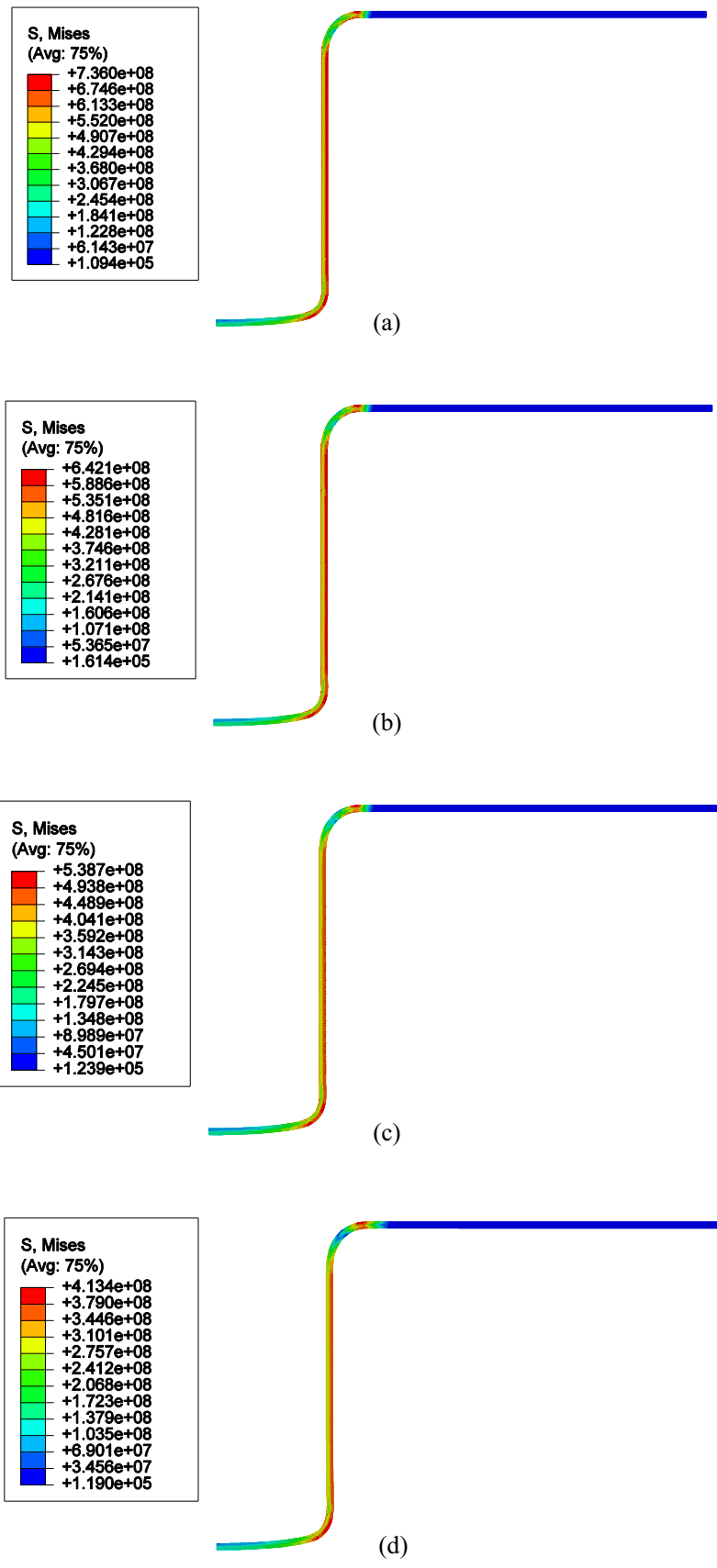
Fig. 11 Distribution of stress for (**a**) $T_h = 100\ °C$, (**b**) $T_h = 200\ °C$, (**c**) $T_h = 300\ °C$, (**d**) $T_h = 400\ °C$ before quenching and after punch stroke

The following constants were determined using JMatPro based on chemical composition [34] as follows: thermal expansion coefficient, linear variation from 1.54×10^{-6}/K at 25 °C to 1.58×10^{-6}/K at 200 °C; heat capacity, linear variation from 0.45 J/gK at 25 °C to 0.52 J/gK at 200 °C; and thermal conductivity, piecewise linear variation of 36.7 W/mK at 25 °C, 36.9 W/mK at 70 °C, 36.8 W/mK at 100 °C, and 36 W/mK at 200 °C. Heat transfer coefficient of metal-air contact is equal to 20 W/m^{2}K and heat transfer coefficient of metal-metal contact is 5 kW/m^{2}K.

6 Contact surfaces

In order to accurate simulation of the hot stamping process, we need to define contact surfaces. Some of these surfaces are in geometrical contact and the others are in thermal contact. There are six contact surfaces as shown in Fig. 4 [13], i.e., (1) geometrical contact surface of die (GCSD), (2)

geometrical contact surface of punch (GCSP), (3) geometrical contact surface of blank holder (GCSBH), (4) upper geometrical contact surface of blank (UGCSB), (5) lower geometrical contact surface of blank (LGCSB), (6) thermal contact surface of blank (TCSB). For each contact surface, the approach of heat transfer is different. The corresponding way of heat transfer from blank to tools can be expressed as follows:

$$q_m = h_{mm}(T - T_1) \qquad (34)$$

where h_{mm} is the heat convection coefficient of metal-metal contact. T_1 is temperature of the tools, T is the temperature of the blank. The equation which describes the heat transfer between the blank to air can be expressed with:

$$q_a = h_{ma}(T - T_\infty) \qquad (35)$$

In the above equation, h_{ma} is the heat convection coefficient between metal and air. Also, T is the blank temperature and T_∞ is the temperature of air.

Fig. 12 **a** Influence of heating temperature on predicted springback profile. **b** Influence of heating temperature on predicted springback parameters

(a)

(b)
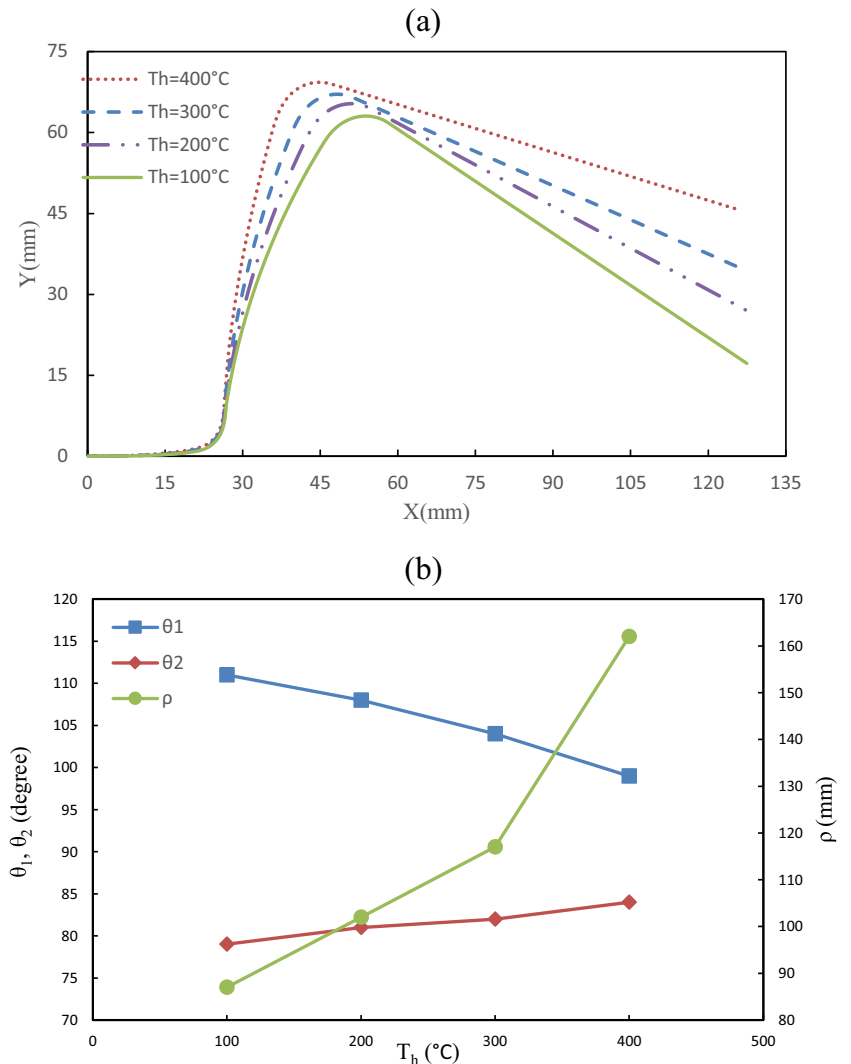
Since the deformations are small in longitudinal direction of the sheet, the position of the points A, B, C, D, E, and F in deformed configuration of the blank in Fig. 4 can be determined in undeformed configuration as shown in Fig. 5. The value of the parameters shown in Fig. 5 are given in the next section.

7 Tooling geometry

A schematic view of tools and their dimensions are shown in Fig. 6. As shown in Table 3, dimensions of the original 2D draw-bending test were slightly modified in order to accommodate the thickness of the new material. The springback parameters which should be measured in the future are shown in Fig. 7.

8 Finite element model

The simulation of finite element bending process is performed in the ABAQUS version 2016 software. Due to the symmetry in the model, only half of the model is simulated. In the case of sheet, CPE4RT (4-node plane strain thermally coupled quadrilateral, bilinear displacement and temperature, reduced integration, hourglass control) element and for punch, holder, and die, the analytical rigid bodies are considered. Surface to surface (Explicit) contact is used to define the contact between the tools and blank. Also, penalty tangential behavior is used to define the friction between the tools and blank. The number of elements in the longitudinal direction is equal to 360 and in the thickness direction of the sheet is equal to 4. The sheet holder force is also considered equal to 2.94 kN. The other parameters which used in hot stamping simulation are summarized in Table 4.

9 Results and discussion

The numerical simulation of the warm U-shaped deep drawing process of DP780 steel sheets was done in the ABAQUS software based on the forward Euler explicit integration scheme. A temperature-dependent Chaboche hardening model and Yld2000-2d yield criterion was used via UMAT and VUMAT user subroutines. In order to validate the present hardening model, a comparison is done with experimental results obtained by [33] in room temperature. The 3D shape of the plate after springback is shown in Fig. 8 a. It can be seen in Fig. 8 b the results obtained based on the Chaboche model have an agreement with experimental data, and the amount of error is represented in Table 5.

Figure 9 shows the distribution of temperature after quenching and before springback for different heating temperatures. It can be seen that the temperature in the area below the

holder is the lowest. Also, the temperature in the side wall area has the least variation. The region below the punch has a little deviate from the punch profile, and so the contact between the punch and this region is not quite established. For this reason, no heat is transferred between these two surfaces and the temperature in this region does not change much.

Figure 10 indicates the effect of temperature at the end of heating process on stress distribution of the sheet at the end of quenching process and after springback. It can be seen that with increasing heating temperature, the stress level at the end of quenching process and after springback decreases, as well as the level of stress after the springback decreases.

Figure 11 reflects the distribution of stress for different heating temperatures after punch stroke and before quenching. By comparing Fig. 10 and Fig. 11, it can be concluded that the level of stress increases after the quenching process.

Figure 12 a and b demonstrate the influence of the heating temperature on predicted springback profile and parameters, respectively. It can be concluded that with increasing the heating temperature, the amount of springback decreases. Also, the heating temperature has the most influence on side-wall curl (ρ) and then θ_1. Heating temperature has the least effect on parameter θ_2.

10 Conclusion

In this paper, the hot stamping process of DP780 steel sheet was simulated based on a novel FE model. For consideration of the hardening behavior of the material, a temperature-dependent Chaboche model and for material anisotropy, Yld2000-2d yield criterion was used. A forming process was simulated in the ABAQUS via the UMAT and VUMAT user subroutines based on the forward Euler explicit integration scheme. The obtained results based on the Chaboche temperature-dependent model had an agreement with experimental results. It was observed that increasing the heating temperature of the sheet causes decreasing the level of stresses. It was seen that the stress level of the sheet after quenching process increases. The distribution of the temperature in region below the holder had the minimum value while the temperature in sidewall and bottom sections of the U-shaped part had the maximum value. Finally, it can be concluded that the amount of springback decreases when heating temperature of the sheet increases.

References

1. Martínez-Palmeth LH, Martínez-Donaire AJ, Vallellano C (2019) Formability limits of high-strength H240LA steel sheets under stress/strain gradients. Mech Mater 132:47–56. https://doi.org/10.1016/j.mechmat.2019.02.014

2. Zhang H, Coppieters S, Jiménez-Peña C, Debruyne D (2019) Inverse identification of the post-necking work hardening behaviour of thick HSS through full-field strain measurements during diffuse necking. Mech Mater 129:361–374. https://doi.org/10.1016/j.mechmat.2018.12.014

3. McDonald B, Bornstein H, Langdon GS, Curry R, Daliri A, Orifici AC (2018) Experimental response of high strength steels to localised blast loading. Int J Impact Eng 115:106–119. https://doi.org/10.1016/j.ijimpeng.2018.01.012

4. He X, Yao Y, Keer LM (2017) A rate and temperature dependent unified creep-plasticity model for high strength steel and solder alloys. Mech Mater 106:35–43. https://doi.org/10.1016/j.mechmat.2017.01.005

5. Zhang Z (2018) Theoretical prediction for maximum residual cross-sectional deformation of thin-walled cylindrical steel tubes under pure plastic bending. Thin-Walled Struct 133:120–133. https://doi.org/10.1016/j.tws.2018.09.004

6. Gan W, Bong HJ, Lim H, Boger RK, Barlat F, Wagoner RH (2017) Mechanism of the Bauschinger effect in Al-Ge-Si alloys. Mater Sci Eng A 684:353–372. https://doi.org/10.1016/j.msea.2016.12.020

7. Kopec M, Wang K, Politis DJ, Wang Y, Wang L, Lin J (2018) Formability and microstructure evolution mechanisms of Ti6Al4V alloy during a novel hot stamping process. Mater Sci Eng A 719:72–81. https://doi.org/10.1016/j.msea.2018.02.038

8. Liu G, Xie J, Xie S (2017) Experimental and numerical investigations of a new U-shaped thin plate energy absorber subjected to bending and friction. Thin-Walled Struct 115:215–224. https://doi.org/10.1016/j.tws.2017.02.025

9. Mori K, Maki S, Tanaka Y (2005) Warm and hot stamping of ultra high tensile strength steel sheets using resistance heating. CIRP Ann - Manuf Technol 54:209–212. https://doi.org/10.1016/S0007-8506(07)60085-7

10. Yanagimoto J, Oyamada K, Nakagawa T (2005) Springback of high-strength steel after hot and warm sheet formings. CIRP Ann - Manuf Technol 54:213–216. https://doi.org/10.1016/S0007-8506(07)60086-9

11. Naderi M, Uthaisangsuk V, Prahl U, Bleck W (2008) A numerical and experimental investigation into hot stamping of boron alloyed heat treated steels. Steel Res Int 79:77–84. https://doi.org/10.1002/srin.200806320

12. Xing ZW, Bao J, Yang YY (2009) Numerical simulation of hot stamping of quenchable boron steel. Mater Sci Eng A 499:28–31

13. Liu HS, Xing ZW, Bao J, Song BY (2010) Investigation of the hot-stamping process for advanced high-strength steel sheet by numerical simulation. J Mater Eng Perform 19:325–334. https://doi.org/10.1007/s11665-009-9510-y

14. Worswick M, Malcolm S, Omer K et al (2017) Testing of a hot stamped axial crush member with tailored properties – experiments and models. Int J Impact Eng 103:12–28. https://doi.org/10.1016/j.ijimpeng.2017.01.003

15. Liu H, Bao J, Xing Z, Zhang D, Song B, Lei C (2011) Modeling and FE simulation of quenchable high strength steels sheet metal hot forming process. J Mater Eng Perform 20:894–902. https://doi.org/10.1007/s11665-010-9713-2

16. Lee JY, Lee MG, Barlat F (2011) Evaluation of constitutive models for springback prediction in U-draw/bending of DP and TRIP steel sheets. AIP Conf Proc 1383:571–578. https://doi.org/10.1063/1.3623659

17. Wei L, Yuying Y, Zhongwen X, Lihong Z (2009) Springback control of sheet metal forming based on the response-surface method and multi-objective genetic algorithm. Mater Sci Eng A 499:325–328. https://doi.org/10.1016/j.msea.2007.11.121

18. Heller B, Kleiner M (2006) Semi-analytical process modelling and simulation of air bending. J Strain Anal Eng Des 41:57–80. https://doi.org/10.1243/030932405X30966

19. Lee M-G, Kim D, Wagoner RH, Chung K (2007) Semi-analytic hybrid method to predict springback in the 2D draw bend test. J Appl Mech 74:1264–1275. https://doi.org/10.1115/1.2745390

20. Panthi SK, Ramakrishnan N (2011) Semi analytical modeling of springback in arc bending and effect of forming load. Trans Nonferrous Met Soc China (English) Ed 21:2276–2284. https://doi.org/10.1016/S1003-6326(11)61008-X

21. Le Quilliec G, Breitkopf P, Roelandt JM, Juillard P (2014) Semi-analytical approach for plane strain sheet metal forming using a bending-under-tension numerical model. Int J Mater Form 7:221–232. https://doi.org/10.1007/s12289-012-1122-7

22. Zhang ZK, Wu JJ, Guo RC, Wang MZ, Li FF, Guo SC, Wang YA, Liu WP (2016) A semi-analytical method for the springback prediction of thick-walled 3D tubes. Mater Des 99:57–67. https://doi.org/10.1016/j.matdes.2016.03.026

23. Hajbarati H, Zajkani A (2018) A novel analytical model to predict springback of DP780 steel based on modified Yoshida-Uemori two-surface hardening model. Int J Mater Form 12:441–455. https://doi.org/10.1007/s12289-018-1427-2

24. Zajkani A, Hajbarati H (2017) Investigation of the variable elastic unloading modulus coupled with nonlinear kinematic hardening in springback measuring of advanced high-strength steel in U-shaped process. J Manuf Process 25:391–401. https://doi.org/10.1016/j.jmapro.2016.12.022

25. Zajkani A, Hajbarati H (2017) An analytical modeling for springback prediction during U-bending process of advanced high-strength steels based on anisotropic nonlinear kinematic hardening model. Int J Adv Manuf Technol 90:349–359. https://doi.org/10.1007/s00170-016-9387-5

26. Chaboche JL (2008) A review of some plasticity and viscoplasticity constitutive theories. Int J Plast 24:1642–1693. https://doi.org/10.1016/j.ijplas.2008.03.009

27. Frederick CO, Armstrong PJ (2007) A mathematical representation of the multiaxial Bauschinger effect. Mater High Temp 24:1–26. https://doi.org/10.3184/096034007X207589

28. Prager W (1949) Recent developments in the mathematical theory of plasticity. J Appl Phys 20:235–241. https://doi.org/10.1063/1.1698348

29. Karvan P, Varvani-Farahani A (2019) Ratcheting assessment of visco-plastic alloys at ambient temperature by means of the A-V and O-W hardening rule frameworks. Mech Mater 130:95–104. https://doi.org/10.1016/j.mechmat.2019.01.007

30. Zhou C, Chen Z, Lee JW, Lee MG, Wagoner RH (2015) Implementation and application of a temperature-dependent Chaboche model. Int J Plast 75:121–140. https://doi.org/10.1016/j.ijplas.2015.03.002

31. Barlat F, Brem JC, Yoon JW, Chung K, Dick RE, Lege DJ, Pourboghrat F, Choi SH, Chu E (2003) Plane stress yield function for aluminum alloy sheets - part 1: theory. Int J Plast 19:1297–1319. https://doi.org/10.1016/S0749-6419(02)00019-0

32. Yoshida F, Uemori T, Fujiwara K (2002) Elastic-plastic behavior of steel sheets under in-plane cyclic tension-compression at large strain. Int J Plast 18:633–659. https://doi.org/10.1016/S0749-6419(01)00049-3

33. Zang SL, Lee MG, Hoon Kim J (2013) Evaluating the significance of hardening behavior and unloading modulus under strain reversal in sheet springback prediction. Int J Mech Sci 77:194–204. https://doi.org/10.1016/j.ijmecsci.2013.09.033

34. Sung JH, Kim JH, Wagoner RH (2010) A plastic constitutive equation incorporating strain, strain-rate, and temperature. Int J Plast 26:1746–1771